





Radiation-based wave-packet generator in one-dimensional lattices

Bastián Real , Diego Guzmán-Silva , and Rodrigo A. Vicencio 

*Departamento de Física, Facultad de Ciencias Físicas y Matemáticas, Universidad de Chile, Santiago 8370448, Chile
and Millenium Institute for Research in Optics - MIRO, Santiago 8370448, Chile*

 (Received 17 August 2023; revised 23 January 2024; accepted 26 January 2024; published 16 February 2024)

The generation of wave packets with well-defined momentum and energy distribution constitutes an experimental challenge in diverse areas of physics. The excitation of nontrivial states, on different lattice configurations, becomes mandatory nowadays to unveil new and exotic properties. In this work, we propose and demonstrate experimentally a straightforward technique to engineer on-chip wave packets by exploiting the radiation of an atomlike waveguide into a one-dimensional lattice. We show that the radiation modes generated after exciting this pseudoatom can be tuned at desired band energies by simply controlling the on-site properties, such that wave packets with precise quasimomentum can be generated. As a benchmark, we use the wave-packet generator for a precise excitation of the well-known topological edge states of a Su-Schrieffer-Heeger photonic lattice.

DOI: [10.1103/PhysRevB.109.064308](https://doi.org/10.1103/PhysRevB.109.064308)

I. INTRODUCTION

Lattice systems are an essential focus of research in physics, with nowadays several experimental configurations devoted to demonstrate their fundamental properties [1–9]. The conceptual idea is essentially the same, to study and control the propagation of waves under restrictions, where photonics has emerged as a key answer for future applications [10–12]. The micrometer scale of typical waveguides makes the observation of different phenomena at hand by using standard optics. Twenty years ago the focus of research in photonics was the demonstration of basic fundamental lattice properties as Bloch modes [13], Bloch oscillations [14], Anderson localization [15,16], among others, but without taking much care about the lattice itself. The last decade, this approach has changed and the studies were focused mostly in the geometrical properties of different lattice configurations [17–19], with a major focus on topology [20–24].

A selective excitation of single states in physical lattices demands a more precise input condition. In optics, standard techniques are based on spatial light modulators (SLMs), which have allowed, for example, a precise excitation of compact states on flatband lattices [18,25–28] or the generation of broad Gaussian beams [27,29,30]. Even though the use of SLMs ensures a fine excitation of specific lattice states, the main drawback is the miniaturization when thinking on on-chip operations beyond photonics. For example, very recently it has been shown numerically [31,32] that a single waveguide can be engineered such that a single-site excitation can pump the topological states of a Su-Schrieffer-Heeger (SSH) lattice [33], showing an alternative route to experimentally overcome the on-chip preparation of a specific light beam. Another way of preparing on-chip beam conditions is, for example, by the addition of defects or impurities. In perfectly periodic lattices, impurities usually produce the appearance of linear bounded/localized states due to a translational symmetry breaking [34,35], with energies lying out

of the bands [36–38]. This is an efficient way of trapping energy at very specific regions of a given lattice, facilitating light guidance [38] and the formation of discrete solitons in nonlinear lattices [39,40].

In this work, by exciting a single defect connected weakly to a one-dimensional (1D) lattice, we demonstrate experimentally the generation of wave packets having a narrow frequency (energy) distribution. When injecting light at the impurity site, a nonbounded mode is excited and the energy radiates into the lattice [36], phenomena that can be interpreted as the radiation of an *atom* into a continuum [41–45]. In this view, the decaying of this atom is essentially exponential for a weak coupling, although the exact form can be more intricate and show different dynamical regimes [46]. We prove that the excitation of the atomlike site dynamically results into the formation of a nonbounded mode, having a large peak at the defect site plus a rather broad propagating wavefront with a very well-defined quasimomentum. Moreover, we show that the nonbounded profile can be tuned in energy and, thus, can resonate with any band state of the 1D lattice. As a proof of concept, we demonstrate that the wave-packet generator can be used to perfectly excite a topological edge state of a SSH lattice. Our results offer a general method to generate on-chip wave packets having a desired quasimomentum (energy), which could be used as a routine technique to excite different states at the interface of any weakly coupled adjacent lattice; namely, compact or edge states in quasi-1D and 2D lattices [19,47,48].

II. MODEL

We study a 1D lattice formed by weakly coupled optical waveguides [40], having a central impurity site as sketched in Fig. 1, top. Gray waveguides form the lattice, while the yellow site represents the impurity or defect waveguide. We consider a separation a_I in between the impurity site and the lattice, and a nominal unit cell lattice distance a . By considering coupled-mode theory [40], which is equivalent to a

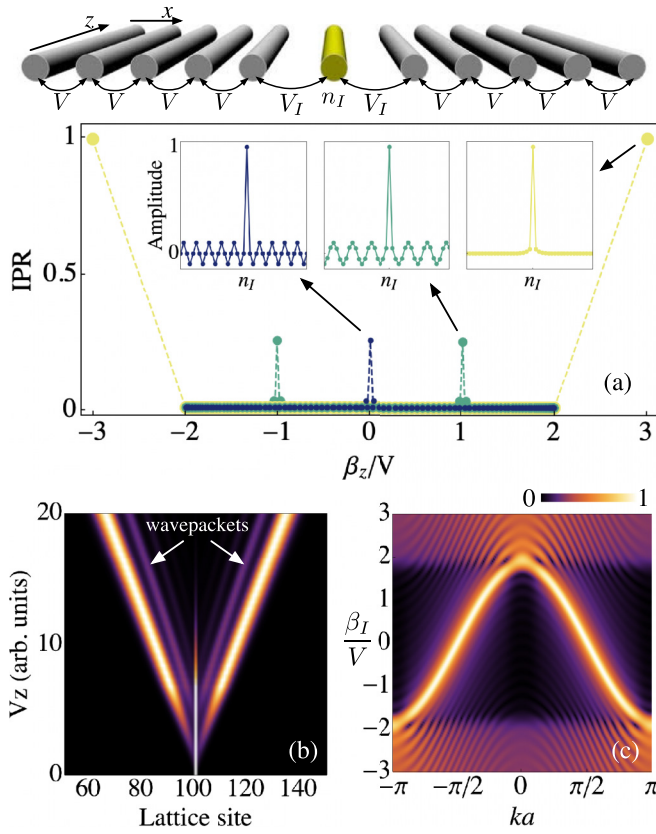


FIG. 1. (Top) Sketch of the wave-packet generator. (a) IPR for all the eigenstates of a 1D lattice with 201 sites and a symmetric coupling defect $V_I/V = 0.1$, for $\beta_I = 0$ (blue), V (green), and $3V$ (yellow). (Insets) Amplitude profiles for the eigenstates with highest IPR, normalized to the largest peak. (b) Intensity profile evolution $|u_n(z)|^2$ for a single-site excitation at the impurity site, and for $\beta_I = 0$. (c) Fourier transform of the amplitude profile at $z_w = 20$ vs the defect detuning β_I/V . In (b) and (c), $V_I = 0.3V$.

tight-binding approach [1], the dynamical equations read as

$$-i \frac{\partial u_n}{\partial z} = \beta_n u_n + \sum_m V_{n,m} u_m. \quad (1)$$

z corresponds to the propagation coordinate along the waveguides, while u_n and β_n represent the mode amplitude and propagation constant (longitudinal frequency) at the n th lattice site, respectively. The lattice structure is defined by the coupling matrix elements $V_{n,m}$, considering the lattice coupling constant V and the coupling of the impurity with the lattice V_I , as described in Fig. 1, top. For a homogeneous 1D lattice (i.e., $\beta_n = \beta_0$ and $V_{n,m} = V \delta_{n,m \pm 1}$), the dispersion relation [40] is given by $\beta_z(k_x) = \beta_0 + 2V \cos(k_x a)$, with k_x the transversal wave vector. For simplicity, we simply set $\beta_0 = 0$. Spatially extended lattice modes have a frequency in the range $[-2V, 2V]$, and a close to zero inverse participation ratio: $\text{IPR} \equiv \sum |\psi_n|^4 / (\sum |\psi_n|^2)^2$, implying delocalization.

Now, we introduce in model (1) the atomlike defect as follows: $\beta_n = \beta_I \delta_{n,n_I}$, with n_I the impurity site, and $V_{n,m} = V + (V_I - V)(\delta_{n,n_I} \delta_{m \pm 1, n_I} + \delta_{n \pm 1, n_I} \delta_{m, n_I})$, for nearest-neighbor sites only ($V_{n,m} = 0$ otherwise). For a perfectly tuned defect ($\beta_I = 0$) and weak coupling ($V_I < V$), a mode with

the highest IPR appears at zero frequency [see blue dots in Fig. 1(a)]. This mode possesses the highest amplitude (A) at the impurity site, and an oscillatory amplitude tail which occupies the rest of the lattice (see blue inset), with a structure given by $A\{\dots, 0, \delta, 0, -\delta, 0, 1, 0, -\delta, 0, \delta, 0, \dots\}$, for $\delta = V_I/V$. Every two lattice sites, a phase difference of π is observed. This corresponds to the phase $k_x a = \pi/2$ of the mid-band eigenstate $\beta_z = 0$ of a 1D lattice. The breaking of the translation symmetry, by the addition of a weakly coupled defect, produces a nonbounded state [36], which is in resonance with the mid-band lattice eigenstate when $\beta_I = 0$. This is in strong contrast with the inclusion of an isolated site impurity ($\beta_I \neq 0$) on a perfectly periodic lattice, that generates a bounded exponential profile with an energy always laying out of the band [35,37,38] and, therefore, never interacting resonantly with a band state.

We numerically integrate model (1) considering a tuned defect ($\beta_I = 0$) and a single-site excitation $u_n(0) = \delta_{n,n_I}$. Figure 1(b) shows that the light propagates initially well confined at the impurity region but, after a given propagation distance [46], most of the light is split into two main opposite wavefronts, which evolve uniformly across the lattice with the highest velocity ($\pm 2V$) [40]. Indeed, a transversal Fourier transform of the amplitude profile $u_n(z_w)$, at a propagation distance z_w , such that the two wavefronts are already generated, reveals that the wavefronts have a very well-defined quasimomentum distribution centered at $\pm\pi/2$ for $\beta_I = 0$, as shown in Fig. 1(c). In practice, a finer tuning of the wave-packet quasimomentum k_x will demand a smaller coupling V_I and, of course, a larger dynamical scale (see Appendix A). The generation of these beams also produces much weaker traveling profiles as the ones shown in Fig. 1(b), inside the cone. These wavefronts travel with a k_x around the main value, but they are too small and negligible in the dynamics as we will show directly in the experiment.

Additionally, we find that the resonance in between the nonbounded excited mode and a given lattice eigenstate occurs at $\beta_z = \beta_I$, with the detuning β_I acting as a control parameter. For example, for $\beta_I = V$, the highest IPR occurs exactly at $\beta_z = V$, as shown in Fig. 1(a). This state has an oscillatory tail with a period of six lattice sites due to the resonance with the $k_x a = \pi/3$ eigenstate (see the green inset profile). As soon as the value of β_I lies within the band range $[-2V, 2V]$, the nonbounded part of the defect mode will predominantly exhibit a phase profile according to the eigenstate it mostly resonates with. Therefore, by changing the defect detuning β_I we can tune this resonance and, as a direct consequence, we can control the central wave-packet quasimomentum k_x . Figure 1(c) shows the Fourier transform of the output amplitude profiles as a function of the detuning β_I/V . For $-2V \leq \beta_I \leq 2V$, the central quasimomentum changes smoothly from $k_x a = \pm\pi$ to 0, passing through $k_x a = \pm\pi/2$ at $\beta_I = 0$. On the other hand, for $|\beta_I| > 2V$ exponentially decaying bound states emerge [35,37,38] with a growing IPR, and with a frequency laying out of the band [36], as the yellow data in Fig. 1(a) shows for $\beta_I = 3V$. The excited spectrum delocalizes for $|\beta_I| > 2V$ [see Fig. 1(c)], as all the states having a non null amplitude at the impurity site are excited, including several extended lattice modes and the bound localized state itself.

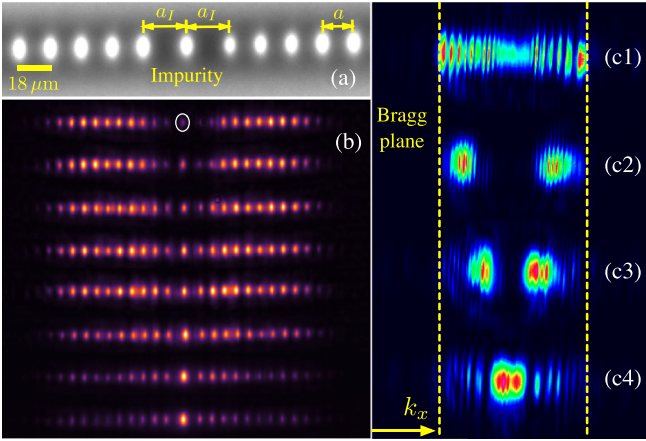


FIG. 2. (a) Output image of a fabricated lattice after white light illumination, with $a = 18$ and $a_I = 26$ μm . (b) Output intensity profiles after a single-site excitation at the impurity site, with P_I increasing downwards. Fourier output intensity profiles for (c1) $V_I = V_I$ and $\Delta P = 0$, and for $V_I < V$ and (c2) $\Delta P = 0$, (c3) 2.25 and (c4) 5.25 mW.

III. EXPERIMENTAL RESULTS

To demonstrate experimentally the radiation-based wave-packet generator, we use the femtosecond (fs) laser writing technique [49,50] to fabricate several 1D photonic lattices having 41 coupled waveguides each, on a 3-cm-long borosilicate glass wafer. Each fabricated waveguide supports a single mode only [51], in the wavelength range under study. The lattice spacing is taken as $a = 18$ μm . Since the coupling constant decays exponentially with the distance [50,51], the coupling impurity ($V_I < V$) is created at the central region by placing the central defect site at $a_I = 26$ μm , with $V = 0.93$ and $V_I = 0.35$ cm^{-1} at 675 nm ($V_I/V \simeq 0.38$). Figure 2(a) shows a microscope image zoom of a fabricated lattice, where the central impurity region is clearly shown. With this technique, the refractive index of every waveguide can be tuned by adjusting the writing power (pulse energy) of the femtosecond laser. This allows us to effectively modify the propagation constant at the impurity site (β_I), which in the experiment corresponds to a refractive index change, as shown in Appendix B. Thus we fabricate 8 different lattices for which the writing power was increased at the central impurity waveguide, in the range $P_I \in \{111, 117\}$ mW, every 0.75 mW. The rest of the lattice waveguides are fabricated using a nominal writing power of $P_0 = 111$ mW. First of all, we test our lattices by using a supercontinuum (SC) laser source at 675 nm. We focus the light beam into the defect waveguide with a 10 \times microscope objective and, then, we observe the near-field intensity of the output facet using a beam profiler. Figure 2(b) shows the output intensity profiles for these 8 lattices, with the writing power P_I increasing downwards. For $\Delta P \equiv P_I - P_0 = 0$ [top figure (b)], the output intensity profile shows two main lobes escaping from the impurity region and, importantly, with almost no light at the impurity site, due to the radiationlike dynamics of a tuned atom [44,46]. This is in perfect agreement with the simulation shown in Fig. 1(b), where the light is radiated into the bulk with two main lobes

traveling at $|k_x a| \approx \pi/2$. We estimate the Gaussian width of this experimental amplitude profile as 5.8, with a participation number $1/IPR = 9.5$. These values were obtained after fitting the experimental profiles to the left and to the right, and then by averaging the respective values. While increasing ΔP , and fixing the wavelength and propagation distance, we notice that the light is less radiated and, also, that the impurity site has an increasing intensity. For the strongest writing power (bottom figure), we detect an intensity profile with most of the light localized at the atom defect plus a weak radiative background. This evidences the formation of a localized bound state with a frequency close to the band upper edge, although its exponential decaying tail is still not completely formed [34,35].

By observing the output intensity at the Fourier plane (far field), we can visualize the excited transversal quasimomentum spectra. This technique has been mostly implemented in photonic for photorefractive SBN induced lattices [40,52], and we are not aware of its use on fs written structures. Figure 2(c1) shows the excited k_x spectrum after injecting light at the central waveguide of a homogeneous 1D lattice ($V_I = V$ and $\beta_I = 0$). We observe that most of the k_x frequencies are excited, up to $k_x \approx \pm\pi/a$ at the Bragg planes [1,40]. In the presence of a coupling impurity only ($V_I < V$ and β_I , $\Delta P = 0$), the Fourier profile in Fig. 2(c2) shows two strong regions centered at $k_x \approx \pm\pi/2a$. This is a confirmation of the predicted generation of two wave packets with a well-defined quasimomentum distribution, centered at the expected k_x values. Figures 2(c3) and 2(c4) show the Fourier profiles considering a coupling defect ($V_I < V$) and a detuned impurity site with $\Delta P = 2.25$ and 5.25 mW, respectively. We detect that the wave-packet quasimomentum distribution shifts to the center, approaching $k_x \sim 0$ at higher ΔP . This observation demonstrates that the coupling impurity creates a nonbounded mode which strongly resonates with a specific band eigenstate and that serves as an on-chip wave-packet generator. Furthermore, the quasimomentum distribution is linked directly to a specific propagation frequency β_z (energy in a time-dependent lattice). Thus we can use this generated wave packet as a precise input condition to excite different eigenstates at adjacent lattices, which could have not only specific energies [53] but also a precise momenta.

We test our method using a standard 1D topological model, the SSH lattice [33]. This lattice is formed by two sublattices, usually called A and B , with different intra- and intercell coupling constants [33,54]. When the intracell coupling is lower than the intercell one, the Zak phase takes a value of π and, consequently, two in-gap edge states exist at zero propagation constant (energy) $\beta_z = 0$. These states decay exponentially from the edge into the bulk, and exhibit the so-called lattice polarization, i.e., the edge state on the left (right) end has amplitudes only at the A (B) sublattice sites. First of all, we realize that only one half of the original wave-packet generator is required to produce a single propagating lobe with a well-defined quasimomentum (see Appendix C). Therefore a weakly coupled tuned atomlike waveguide [at the left edge in this case, as shown in Fig. 3(a), top] will be able to generate a wave packet with a quasimomentum centered at $k_x = \pi/2a$ (in this case, the diffraction coefficient is zero [40] and, therefore, we expect a direct interaction in between the beam and the SSH lattice). This time, we fabricate our system on a

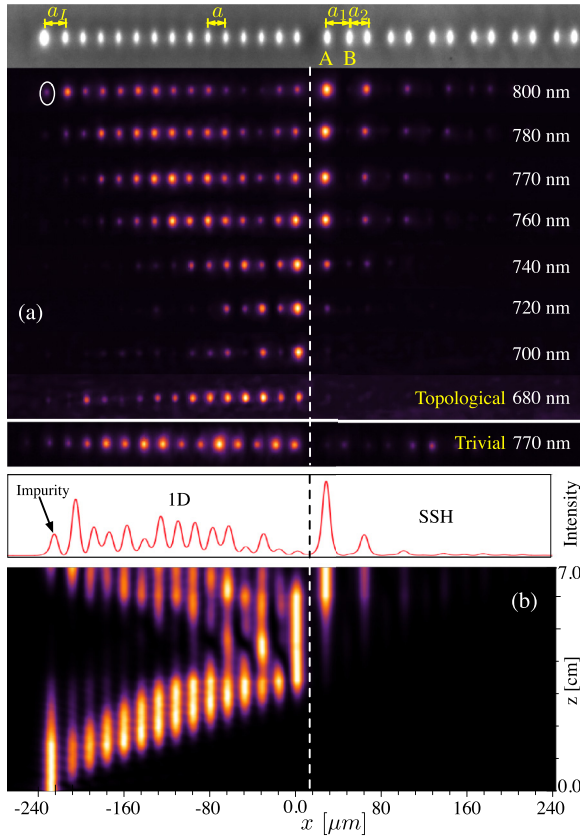


FIG. 3. Precise excitation of a SSH edge state by means of the wave-packet generator. (Top) Output image of the lattice system under study after white illumination. (a) Experimental output intensity profiles at different wavelengths, after exciting the waveguide impurity (ellipse). (b) Numerical intensity profiles vs z , for a beam at 760 nm, after a Gaussian input excitation at the impurity site. The top panel in (b) shows a normalized intensity profile at $z = 7$ cm. The dashed vertical lines indicate the interface in between the 1D and the SSH lattices $a = 18$ and $a_l = 26$ μm .

7-cm-long glass wafer, due to the requirement of having a larger propagation distance to first generate the wave packet and, then, to excite the SSH lattice system. A tuned impurity waveguide is placed at a distance $a_l = 19$ μm ($V = 0.82$ cm^{-1} at 675 nm) apart from a 1D photonic lattice having a lattice period of $a = 16$ μm ($V = 1.17$ cm^{-1} at 675 nm). The intra- and intercell distances, of the SSH lattice at the right, are taken as $a_1 = 21$ μm and $a_2 = 16$ μm ($V_1 = 0.65$ and 1.17 cm^{-1} at 675 nm), respectively, such that we are in a topologically nontrivial phase regime [31,32]. We consider a weak coupling $V = 0.31$ cm^{-1} (separation of 27 μm) in between the 1D and the SSH lattices, such that both systems can be treated as two independent ones; otherwise, interface states could appear and disrupt the excitation. All the waveguides are fabricated using the same writing power 111 mW, such that we can generate a wave packet $k_x = +\pi/2a$ at zero energy.

We use a SC laser source to excite the impurity atom at different wavelengths in the range $\lambda \in \{680, 800\}$ nm. Different colors allow us to emulate different propagation distances [55–57], as the coupling constants increase almost linearly with λ [48]. Figure 3(a) shows very clearly the effective

dynamics in the system, after exciting the impurity site with different wavelengths. For the shortest wavelength of 680 nm (bottom), the output intensity profile shows that the wave packet has been generated [similar to Fig. 2(b), top] and is traveling to the interface region (dashed line). Then, the wave packet interacts with the interface at a wavelength of ~ 700 –720 nm, where some light is also reflected back. For longer wavelengths, we first observe how the reflected light continues traveling smoothly to the left. More importantly, the light that is transmitted to the right, into the SSH lattice, starts to occupy mostly the waveguides belonging to the sublattice A and, very remarkably indeed, the intensity profile exhibits a perfect exponential decaying tendency (we obtained similar results for SSH lattices having weaker dimerizations and holding edge states with larger localization lengths, as shown in Appendix D). By repeating the same experiment but, now, considering a SSH lattice with a trivial (opposite) dimerization $a_1 = 16$ μm and $a_2 = 21$ μm , almost no transmitted light is detected to the right due to the absence of any state to excite at zero frequency [33] [see an example in Fig. 3(a), bottom, and more details in Appendix D]. Moreover, when modifying slightly the impurity frequency β_l we observe a non optimal transmission of light beyond the interface (see Appendix D), because the quasimomentum of the generated wave packet has changed and its energy lies now in the SSH band gap. It is worth mentioning that a single site excitation at the edge of a SSH lattice also excites the edge states [47,58,59]. However, its efficiency strongly depends on the dimerization contrast (a_2/a_1) and, also, on the propagation length because all eigenstates with nonzero amplitude at the excitation site will be excited. Conversely, our method enables a rather pure and coherent excitation of the edge states at a selected energy.

Finally, we support our experimental results using continuous numerical simulations. We use a beam propagation method (BPM) to obtain the dynamics along the propagation coordinate z for a Gaussian beam excitation at 760 nm (more details in Appendix B). We study a paraxial wave equation [18] and consider a refractive index profile similar to the experimental one, with a nominal refractive index $n_0 = 1.48$ and a waveguide contrast of 1.5×10^{-4} . Figure 3(b) shows our results with a clear wave packet generated into the right direction, after the excitation of the impurity site. Then, the light travels transversally across the 1D homogeneous lattice and reaches the interface with the SSH system at $z \sim 4$ cm. There, we notice an interference pattern similar to the one observed in the experiment at ~ 700 –720 nm, which is characteristic for $k_x = \pm\pi/2a$ waves. At larger distances, some light is transmitted and excites, quite precisely indeed, a localized profile at the left edge of the SSH lattice. The top panel in Fig. 3(b) shows a normalized intensity profile at 7 cm of propagation, where an exponentially decaying topological profile, with nonzero amplitudes every two lattice sites, is clearly formed.

IV. CONCLUSIONS

In conclusion, we have proposed an experimental technique to create on-chip wave packets with a precise quasimomentum control, using a simple single-site lattice excitation. This exploits the properties of nonbounded modes excited

on a 1D lattice having a weakly coupled waveguide, which behaves as an impurity radiating atom. We have experimentally demonstrated this concept on femtosecond-laser written photonic lattices and characterize it by means of a SC laser source. We probe our method on the iconic 1D SSH topological lattice and observe both, numerically and experimentally, a quite pure excitation of a localized topological edge state at zero propagation constant (energy). Our new technique simplifies enormously the external creation of an input beam having a given momentum/energy distribution, using just a single-site excitation. Furthermore, we envision an active control of the on-site frequency at the impurity site either by injecting a pulsed laser and, thus, triggering nonlinear effects [50], or by including a metal layer on top and then applying an external DC field [60,61].

ACKNOWLEDGMENTS

The authors acknowledge fruitful discussions with P. Solano and financial support by Millennium Science Initiative Program ICN17_012, and FONDECYT Grant No. 1231313. B.R. acknowledges financial support by ANID FONDECYT de postdoctorado No. 3230139.

APPENDIX A: NUMERICAL STUDY OF THE ATOMLIKE DEFECT

We study numerically the atomlike defect in a 1D lattice. Specifically, we integrate Eq. (1) considering a 1D lattice composed of 201 sites, with the atomlike defect placed at site 101, and a propagation length of $z = 20$. For each propagation, we control both the on-site and the coupling terms of the atomlike site: β_I and V_I , respectively. Firstly, we study the impact of the on-site term on the generated wave packets for a fixed value of V_I . Figure 4(a) shows a density plot for the output intensities ($|u_n(20)|^2$) after exciting the defect, while sweeping β_I within the range $\{0, 3V\}$ and for $V_I = 0.3V$ (V is the lattice coupling). We observe that the two opposite generated wave packets reach a maximum transversal distance, from the atomlike site, for $\beta_I = 0$. For $0 < \beta_I < 2V$, the wave packets travel a shorter distance because the impurity resonates with band modes that have a lower group velocity, as shown in Fig. 1(c). For $\beta_I \geq 2V$, the output intensity exhibits a localized-like profile because the on-site term β_I is out of the band, and there is no available modes to resonate with (the same behavior is observed for negative values of β_I). Secondly, we investigate the effect of V_I on the transversal wave vector (quasimomentum) of the generated wave packet. To do this, we set $\beta_I = 0$ and we vary V_I from 0 to $3V$. For $V_I \lesssim 0.2V$, Fig. 4(b) shows a quite localized profile because the atomlike site is extremely weakly coupled to the lattice and much longer distances are needed to observe radiation to the system. However, once V_I increases, all the light injected into the atomlike defect travels to the lattice possessing a very well defined profile and quasimomentum. This is validated by calculating the Fourier transform of Fig. 4(b), as it is shown in Fig. 4(c). We can clearly see that a narrower quasimomentum width is obtained only for $V_I < 0.5V$. As soon as V_I approaches V , the wave packets become broader in real space (covering more lattice sites with nonzero amplitudes),

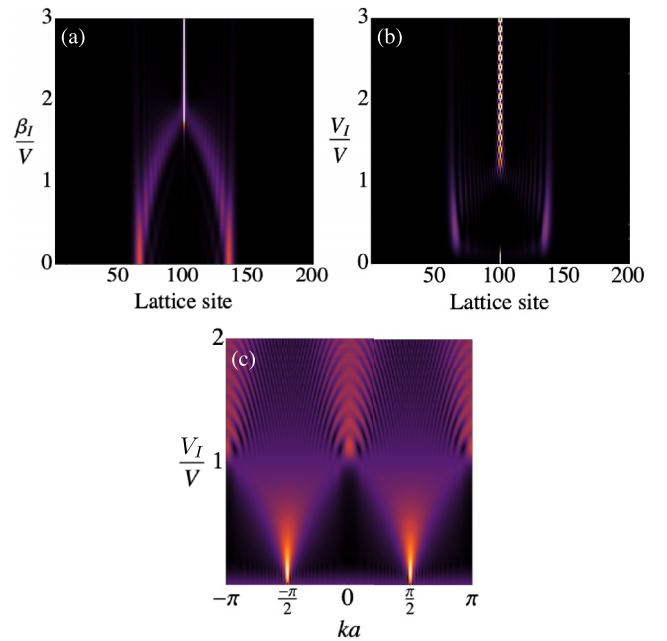


FIG. 4. Simulation of an atomlike impurity or defect in a 1D lattice. (a) Density plot of the simulated output intensities for $V_I = 0.3V$ and β_I in the range $[0, 3V]$. (b) Density plot of the simulated output intensities for $\beta_I = 0$ and V_I in the range $[0, 3V]$. (c) Fourier transform of the output amplitude for $\beta_I = 0$ and V_I in the range $[0, 3V]$. The 1D lattice is composed of 201, the impurity is placed at the site 101, and the propagation length is $z = 20$.

and get a wider and not well defined transversal wave-vector distribution. For $V_I = V$, there is no defect at all and a typical discrete diffraction pattern is observed. For $V_I > V$, a caging effect is observed in between two localized states, as it is shown in Fig. 4(b).

APPENDIX B: SIMULATION BASED ON BPM

Light propagation through an optical media can be described by a paraxial wave equation of the form

$$-i \frac{\partial}{\partial z} \Psi(x, y, z) = \frac{\nabla_{\perp}^2 \Psi(x, y, z)}{2k_o n_o} + k_o \Delta n(x, y) \Psi(x, y, z),$$

where $\Psi(x, y, z)$ is the electric field amplitude, z is the propagation coordinate, x and y are the transversal coordinates, $k_o = 2\pi/\lambda$ the wave number in free space, λ the wavelength, and n_o the bulk refractive index. $\nabla_{\perp}^2 = \partial_x^2 + \partial_y^2$ corresponds to the transversal Laplacian operator, while $\Delta n(x, y)$ defines the transversal refractive index structure fabricated inside the material. Numerical integration of this equation is implemented by means of a beam propagation method (BPM) [62,63], where we numerically simulate the propagation of an initial profile through a given optical media. In order to initialize the simulation, we set some optical parameters according to the real parameters used in the experiment. In this case, we used $\lambda = 675$ nm, bulk refractive index $n_o = 1.48$ and an optical lattice with a period of $18 \mu\text{m}$ plus a central defect with a distance of $26 \mu\text{m}$, which are the same values used in Fig. 2. The shape of the waveguides follows an elliptical profile $\Delta n \tanh[1/(\exp(x/\omega_x)^2 + \exp(y/\omega_y)^2)]$, with $\omega_x = 21 \mu\text{m}$

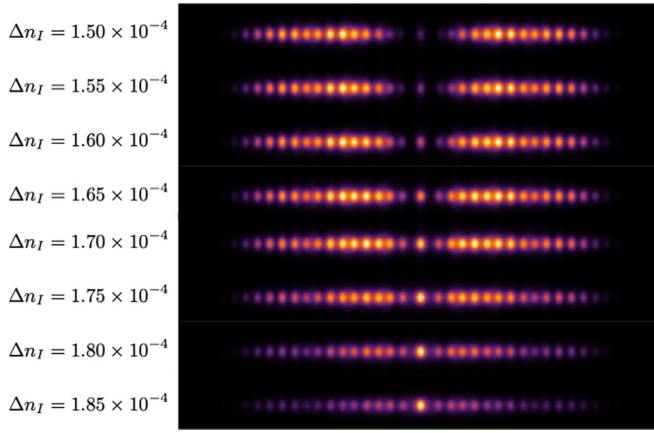


FIG. 5. Numerically computed output intensity profiles after 3 cm of propagation for different values of Δn_I .

and $\omega_y = 40 \mu\text{m}$. The results, using an input beam injected at the defect site and a propagation of 3 cm, are shown in Fig. 5. There, $\Delta n = 1.5 \times 10^{-4}$ for the waveguides along the array, while for the defect site Δn_I was changed linearly from 1.5 to 1.85×10^{-4} , in steps of 0.05×10^{-4} . This linear change in the refractive index was used due to the linear increment of the writing power used in the experiment. We observe an excellent agreement between simulation and experimental results, when comparing Figs. 2(b) and 5. Figure 3(b) was obtained using the same numerical configuration.

APPENDIX C: ATOMLIKE DEFECT PLACED AT THE LATTICE BORDER

The radiation generated by the atomlike defect placed in the middle of the 1D lattice can also be observed when locating this defect at either border of the lattice [42]. Figure 6-Top

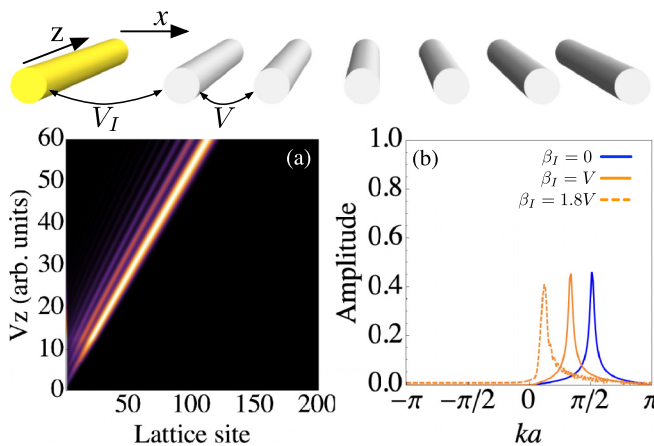


FIG. 6. Simulation of an atomlike impurity or defect at one edge of a 1D lattice. (a) Density plot of the simulated dynamics for $V_I = 0.3V$ and $\beta_I = 0$. (b) Fourier transform of the output amplitude ($z = 60$) for $\beta_I = 0$ (blue curve), V (orange curve) and $1.8V$ (dashed orange curve). The 1D lattice is composed of 201 sites and the impurity is placed on the site 1.

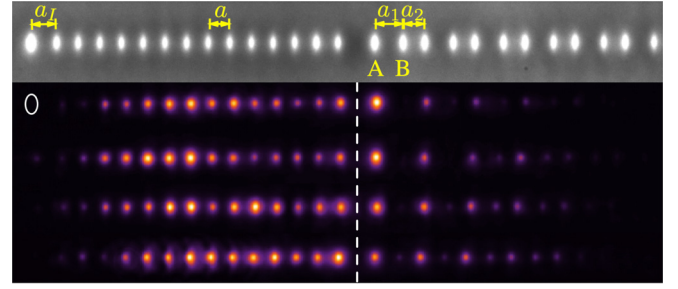


FIG. 7. Excitation of the SSH edge state for several intercell distances ($a_1 = 21, 20, 19, 18 \mu\text{m}$ from top to bottom) and fixed intracell one ($a_2 = 16 \mu\text{m}$) by using the generated wave packet. The atomlike defect is placed on the left side of the 1D lattice at a distance $a_I = 19 \mu\text{m}$ (white ellipse) and it is excited with a SC laser at $\lambda = 770 \text{ nm}$. The lattices are separated by $27 \mu\text{m}$.

depicts the case when an atomlike waveguide is placed at the left side of a 1D photonic lattice. We integrated numerically Eq. (1) using a single site excitation of the form $u_n(0) = \delta_{n,1}$ and considering $\beta_I = 0$. The simulated dynamics is shown in Fig. 6(a). We observe that all the injected light is transferred to the 1D lattice and, at $z_f = 60$, no light can be seen at the atomlike waveguide. Performing a Fourier transform of the amplitude profile at z_f , we retrieved the transversal wave vector of this radiation, which is shown by the blue curve in Fig. 6(b). As expected, the peak of the quasimomentum is centered at $ka = \pi/2$ without appreciable background. Therefore a wave packet with a well-defined quasimomentum distribution is also observed in this configuration. If the on-site term β_I is increased, the wave packet changes its transverse wave vector towards a zero value, as shown by the dashed and continuum orange curves in Fig. 6(b). When β_I approaches $2V$, an oscillatory decay of the quasimomentum distribution is observed, which may impact the pure excitation of a desired state on a given adjacent lattice.

APPENDIX D: ADDITIONAL EXPERIMENTAL RESULTS

1. Excitation of the topological edge state for several dimerized SSH lattices

In this section, we show additional experimental results for the lattice system described in Fig. 3, but with different intercell distances. Specifically, we fabricated systems formed by a 1D lattice which is weakly coupled to a topological SSH lattice (as the one shown in Fig. 7, top). The atomlike defect was placed always at the left side at a distance $a_I = 19 \mu\text{m}$, and the separation distance in between both lattices was set to $27 \mu\text{m}$. We reduced the intracell distance a_1 from 21 to $18 \mu\text{m}$, which results on an increment of the intercell coupling from 0.65 to 0.94 cm^{-1} , at 775 nm . Figure 7 shows the obtained output intensities after 7 cm of propagation, after exciting the atomlike defect with the SC laser at 770 nm . Importantly, we observe that the light is mostly located at the sublattice A. Moreover, the exponential tail of the edge state penetrates deeper into the bulk of the SSH lattice as the intercell distance (coupling) is reduced (increased), which is expected

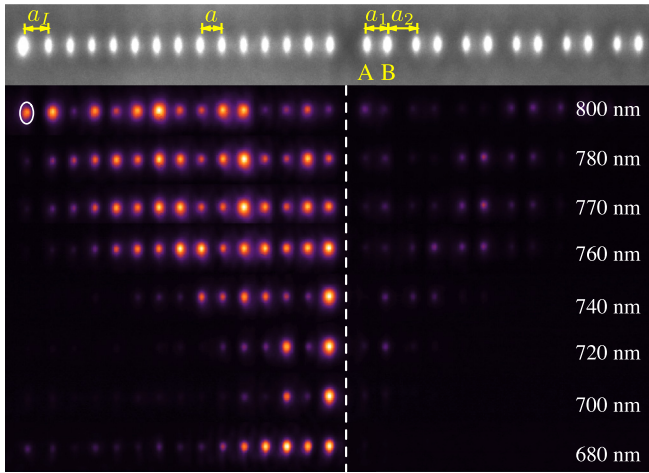


FIG. 8. Output intensity profiles of a lattice system composed of a 1D photonic lattice weakly coupled to a trivial SSH lattice on the right, and an atomlike defect on the left side. Parameters of the lattice system are given in the text.

from a reduction of the dimerization. We can see also some light at the sublattice B for the weakest dimerization ($a_1 = 18 \mu\text{m}$ and $a_2 = 16 \mu\text{m}$), because the width of the wave-packet quasimomentum becomes wider than the SSH band gap and, thus, some bulk modes could be excited weakly.

2. 1D photonic lattice with an atomlike defect weakly coupled to a trivial SSH lattice

We then probed experimentally the case of a 1D photonic lattice with an atomlike defect that is weakly coupled to a trivial SSH lattice. We used a 7-cm-long glass wafer to fabricate a 1D photonic lattice having a lattice constant of $16 \mu\text{m}$ ($V = 1.17 \text{ cm}^{-1}$ at 675 nm). We placed the impurity on the left side of the lattice at a distance of $19 \mu\text{m}$ ($V_1 = 0.82 \text{ cm}^{-1}$ at 675 nm), as sketched in Fig. 8, top. On the right side of the 1D lattice, we fabricated a trivial SSH lattice at a distance of $27 \mu\text{m}$ (coupling of 0.35 cm^{-1} at 675 nm), which has intra- and intercell distances of $a_1 = 16 \mu\text{m}$ and $a_2 = 21 \mu\text{m}$ ($V_1 = 1.17$ and $V_2 = 0.65 \text{ cm}^{-1}$ at 675 nm), respectively. In the experiment, we inject light coming from a supercontinuum laser onto the impurity atom at several wavelengths in the range $\{680, 800\} \text{ nm}$, allowing us to explore the effective lattice dynamics as we were observing at longer propagation distances [48]. Figure 8 displays the output intensity profiles after 7 cm of propagation. For the shorter wavelengths ($\lambda < 720 \text{ nm}$), we observe a traveling wave packet moving towards the interface denoted by the vertical dashed line. At 740 nm , most of the light is reflected back by the interface, with a very weak intensity leaking to the trivial SSH lattice. For longer wavelengths, the output intensity profiles show that almost no light is found in the SSH lattice and the wave packet is mostly traveling back across the 1D photonic lattice, reaching the atom impurity at 800 nm . This observation confirms the absence of edge states in the trivial SSH lattice and, also, that the wave packet encodes a specific energy value inside the gap of the SSH lattice, because almost no light is effectively transmitted.

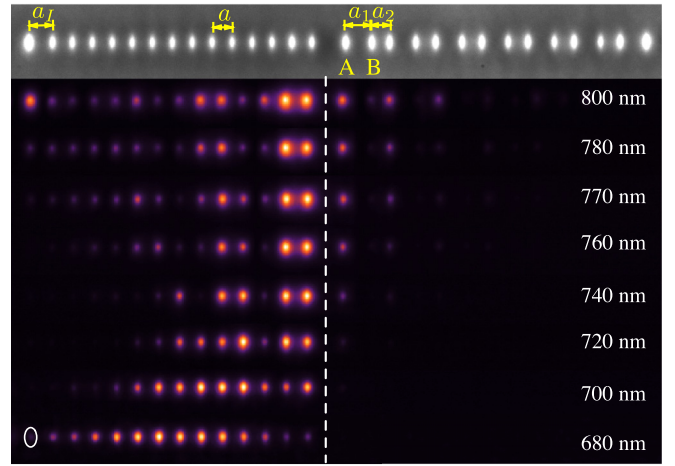


FIG. 9. Output intensity profiles of a lattice system composed of a 1D photonic lattice weakly coupled to a SSH lattice on the right and a detuned atomlike defect on the left side. The writing power difference between the detuned atomlike waveguide and the other waveguides is $\Delta P = 75 \text{ mW}$.

3. 1D photonic lattice with a detuned atomlike defect weakly coupled to a topological SSH lattice

Figure 2 shows that the manipulation of the writing power at the defect waveguide enables a fine tune of the wave-packet quasimomentum and, thus, of the wave-packet energy. Now, we demonstrate experimentally that a detuned atomlike waveguide generates a wave packet which encodes a nonzero energy. Again, we fabricated a 1D lattice which is weakly coupled to a topological SSH lattice at the right side, with a detuned atomlike waveguide at the left side on a 7-cm-long wafer. Specifically, lattice constant of the 1D lattice is $a = 16 \mu\text{m}$, inter- and intracell distances of the SSH lattice are $a_1 = 21 \mu\text{m}$ and $a_2 = 16 \mu\text{m}$, and the separation among the lattices is $27 \mu\text{m}$ (coupling values are the same given in previous section). The atomlike waveguide was placed at $a_1 = 19 \mu\text{m}$ far from the left side of the 1D lattice and, in order to detune it, we increased its fabrication power by 0.75 mW . Figure 9, top, shows a microscopic image of output facet of this lattice system, in which leftmost bright ellipse corresponds to the atomlike waveguide. To reveal the dynamics along the waveguides, we used a SC laser to shine the atomlike waveguide and we observed the output intensities at a fixed propagation length of 7 cm. As it was described in previous section, the light travels towards the interface for wavelengths shorter than 740 nm , as shown in Fig. 9. For longer wavelengths, most of the light is reflected back to the 1D photonic lattice and appreciable light gets transmitted. This transmitted light occupies preferentially the A sublattices implying the presence of the SSH edge state. However, we notice that, in this case, the edge states are only weakly excited, compared to the tuned excitation shown in Figs. 3(a) and 7. The coupling ratio $V_1/V \simeq 0.7$ produces a wave packet with a broad quasimomentum distribution [see Fig. 4(c)] and, therefore, although the wave packet possesses a central energy shifted from zero, it also encodes some energies around this value.

- [1] C. Kittel, *Introduction to Solid State Physics*, 7th ed. (Wiley, New York, 1996).
- [2] M. Sato and A. J. Sievers, Driven localized excitations in the acoustic spectrum of small nonlinear macroscopic and microscopic lattices, *Phys. Rev. Lett.* **98**, 214101 (2007).
- [3] S. Butz, P. Jung, L. V. Filippenko, V. P. Koshelets, and A. V. Ustinov, A one-dimensional tunable magnetic metamaterial, *Opt. Express* **21**, 22540 (2013).
- [4] J. H. Denschlag, BEC in a lattice: Early experiments, *J. Phys. B: At. Mol. Opt. Phys.* **49**, 220502 (2016).
- [5] A. Amo and J. Bloch, Exciton-polaritons in lattices: A nonlinear photonic simulator, *C. R. Phys.* **17**, 934 (2016).
- [6] M. J. A. Schuetz, J. Knörzer, G. Giedke, L. M. K. Vandersypen, M. D. Lukin, and J. I. Cirac, Acoustic traps and lattices for electrons in semiconductors, *Phys. Rev. X* **7**, 041019 (2017).
- [7] Z. Liu, Z. Yang, X. Chen, R. Tan, G. Li, Z. Gan, Y. Shao, J. He, Z. Zhang, W. Li, W.-B. Zhang, and X.-H. Dong, Discrete giant polymeric chains based on nanosized monomers, *JACS Au* **1**, 79 (2021).
- [8] S. Wang, G. Zhang, X. Wang, Q. Tong, J. Li, and G. Ma, Spin-orbit interactions of transverse sound, *Nat. Commun.* **12**, 6125 (2021).
- [9] A. Chen, H. Brand, T. Helbig, T. Hofmann, S. Imhof, A. Fritzsche, T. Kießling, A. Stegmaier, L. K. Upreti, T. Neupert, T. Bzdušek, M. Greiter, R. Thomale, and I. Boettcher, Hyperbolic matter in electrical circuits with tunable complex phases, *Nat. Commun.* **14**, 622 (2023).
- [10] M. Lipson, Guiding, modulating, and emitting light on silicon—challenges and opportunities, *J. Lightwave Technol.* **23**, 4222 (2005).
- [11] J. Wang, F. Sciarrino, A. Laing, and M. G. Thompson, Integrated photonic quantum technologies, *Nat. Photon.* **14**, 273 (2020).
- [12] G. Genty, L. Salmela, J. M. Dudley, D. Brunner, A. Kokhanovskiy, S. Kobtsev, and S. K. Turitsyn, Machine learning and applications in ultrafast photonics, *Nat. Photon.* **15**, 91 (2021).
- [13] D. Mandelik, H. S. Eisenberg, Y. Silberberg, R. Morandotti, and J. S. Aitchison, Band-gap structure of waveguide arrays and excitation of Floquet-Bloch solitons, *Phys. Rev. Lett.* **90**, 053902 (2003).
- [14] R. Morandotti, U. Peschel, J. S. Aitchison, H. S. Eisenberg, and Y. Silberberg, Experimental observation of linear and nonlinear optical Bloch oscillations, *Phys. Rev. Lett.* **83**, 4756 (1999).
- [15] T. Schwartz, G. Bartal, S. Fishman, and M. Segev, Transport and Anderson localization in disordered two-dimensional photonic lattices, *Nature (London)* **446**, 52 (2007).
- [16] Y. Lahini, A. Avidan, F. Pozzi, M. Sorel, R. Morandotti, D. N. Christodoulides, and Y. Silberberg, Anderson localization and nonlinearity in one-dimensional disordered photonic lattices, *Phys. Rev. Lett.* **100**, 013906 (2008).
- [17] C. E. Rüter, K. G. Makris, R. El-Ganainy, D. N. Christodoulides, M. Segev, and D. Kip, Observation of parity–time symmetry in optics, *Nat. Phys.* **6**, 192 (2010).
- [18] R. A. Vicencio, C. Cantillano, L. Morales-Inostroza, B. Real, C. Mejía-Cortés, S. Weimann, A. Szameit, and M. I. Molina, Observation of localized states in Lieb photonic lattices, *Phys. Rev. Lett.* **114**, 245503 (2015).
- [19] S. Stützer, Y. Plotnik, Y. Lumer, P. Titum, N. H. Lindner, M. Segev, M. C. Rechtsman, and A. Szameit, Photonic topological Anderson insulators, *Nature (London)* **560**, 461 (2018).
- [20] A. B. Khanikaev, S. Hossein Mousavi, W.-K. Tse, M. Kargarian, A. H. MacDonald, and G. Shvets, Photonic topological insulators, *Nat. Mater.* **12**, 233 (2013).
- [21] M. Hafezi, S. Mittal, J. Fan, A. Migdall, and J. M. Taylor, Imaging topological edge states in silicon photonics, *Nat. Photon.* **7**, 1001 (2013).
- [22] Y. Plotnik, M. C. Rechtsman, D. Song, M. Heinrich, J. M. Zeuner, S. Nolte, Y. Lumer, N. Malkova, J. Xu, A. Szameit, Z. Chen, and M. Segev, Observation of unconventional edge states in ‘photonic graphene’, *Nat. Mater.* **13**, 57 (2014).
- [23] S. Barik, H. Miyake, W. DeGottardi, E. Waks, and M. Hafezi, Two-dimensionally confined topological edge states in photonic crystals, *New J. Phys.* **18**, 113013 (2016).
- [24] T. Ozawa, H. M. Price, A. Amo, N. Goldman, M. Hafezi, L. Lu, M. C. Rechtsman, D. Schuster, J. Simon, O. Zilberberg, and I. Carusotto, Topological photonics, *Rev. Mod. Phys.* **91**, 015006 (2019).
- [25] Y. Zong, S. Xia, L. Tang, D. Song, Y. Hu, Y. Pei, J. Su, Y. Li, and Z. Chen, Observation of localized flat-band states in Kagome photonic lattices, *Opt. Express* **24**, 8877 (2016).
- [26] B. Real, C. Cantillano, D. López-González, A. Szameit, M. Aono, M. Naruse, S.-J. Kim, K. Wang, and R. A. Vicencio, Flat-band light dynamics in Stub photonic lattices, *Sci. Rep.* **7**, 15085 (2017).
- [27] S. Xia, A. Ramachandran, S. Xia, D. Li, X. Liu, L. Tang, Y. Hu, D. Song, J. Xu, D. Leykam, S. Flach, and Z. Chen, Unconventional flatband line states in photonic Lieb lattices, *Phys. Rev. Lett.* **121**, 263902 (2018).
- [28] J. Ma, J.-W. Rhim, L. Tang, S. Xia, H. Wang, X. Zheng, S. Xia, D. Song, Y. Hu, Y. Li, B.-J. Yang, D. Leykam, and Z. Chen, Direct observation of flatband loop states arising from nontrivial real-space topology, *Phys. Rev. Lett.* **124**, 183901 (2020).
- [29] F. Diebel, D. Leykam, S. Kroesen, C. Denz, and A. S. Desyatnikov, Conical diffraction and composite Lieb bosons in photonic lattices, *Phys. Rev. Lett.* **116**, 183902 (2016).
- [30] C. Cantillano, L. Morales-Inostroza, B. Real, S. Rojas-Rojas, A. Delgado, A. Szameit, and R. A. Vicencio, Observation of dipolar transport in one-dimensional photonic lattices, *Sci. Bull.* **62**, 339 (2017).
- [31] D. Viedma, G. Queraltó, J. Mompert, and V. Ahufinger, High-efficiency topological pumping with discrete supersymmetry transformations, *Opt. Express* **30**, 23531 (2022).
- [32] D. Viedma, J. Mompert, and V. Ahufinger, Mode pumping in photonic lattices using a single tailored auxiliary waveguide, *Phys. Rev. A* **107**, 023506 (2023).
- [33] P. Delplace, D. Ullmo, and G. Montambaux, Zak phase and the existence of edge states in graphene, *Phys. Rev. B* **84**, 195452 (2011).
- [34] G. Leibfried and N. Breuer, Transition from lattice to continuum theory, in *Point Defects in Metals I*, Springer Tracts in Modern Physics Vol. 81 (Springer, Berlin, Heidelberg, 1978), pp. 186–237.
- [35] M. I. Molina, L. Q. English, M.-H. Chang, and P. G. Kevrekidis, Linear impurity modes in an electrical lattice: Theory and experiment, *Phys. Rev. E* **100**, 062114 (2019).
- [36] H. Trompeter, U. Peschel, T. Pertsch, F. Lederer, U. Streppel, D. Michaelis, and A. Bräuer, Tailoring guided modes in waveguide arrays, *Opt. Express* **11**, 3404 (2003).

- [37] X. Wang, J. Young, Z. Chen, D. Weinstein, and J. Yang, Observation of lower to higher bandgap transition of one-dimensional defect modes, *Opt. Express* **14**, 7362 (2006).
- [38] I. Makasyuk, Z. Chen, and J. Yang, Band-gap guidance in optically induced photonic lattices with a negative defect, *Phys. Rev. Lett.* **96**, 223903 (2006).
- [39] Y. Li, W. Pang, Y. Chen, Z. Yu, J. Zhou, and H. Zhang, Defect-mediated discrete solitons in optically induced photorefractive lattices, *Phys. Rev. A* **80**, 043824 (2009).
- [40] F. Lederer, G. I. Stegeman, D. N. Christodoulides, G. Assanto, M. Segev, and Y. Silberberg, Discrete solitons in optics, *Phys. Rep.* **463**, 1 (2008).
- [41] L. E. F. Foa Torres, H. M. Pastawski, and S. S. Makler, Tuning a resonance in fock space: Optimization of phonon emission in a resonant-tunneling device, *Phys. Rev. B* **64**, 193304 (2001).
- [42] S. Longhi, Nonexponential decay via tunneling in tight-binding lattices and the optical zeno effect, *Phys. Rev. Lett.* **97**, 110402 (2006).
- [43] P. Biagioni, G. D. Valle, M. Ornigotti, M. Finazzi, L. Duò, P. Laporta, and S. Longhi, Experimental demonstration of the optical Zeno effect by scanning tunneling optical microscopy, *Opt. Express* **16**, 3762 (2008).
- [44] F. Dreisow, A. Szameit, M. Heinrich, T. Pertsch, S. Nolte, A. Tünnermann, and S. Longhi, Decay control via discrete-to-continuum coupling modulation in an optical waveguide system, *Phys. Rev. Lett.* **101**, 143602 (2008).
- [45] K. Sinha, P. Meystre, E. A. Goldschmidt, F. K. Fatemi, S. L. Rolston, and P. Solano, Non-Markovian collective emission from macroscopically separated emitters, *Phys. Rev. Lett.* **124**, 043603 (2020).
- [46] A. Crespi, F. V. Pepe, P. Facchi, F. Sciarrino, P. Mataloni, H. Nakazato, S. Pascazio, and R. Osellame, Experimental investigation of quantum decay at short, intermediate, and long times via integrated photonics, *Phys. Rev. Lett.* **122**, 130401 (2019).
- [47] G. Cáceres-Aravena, B. Real, D. Guzmán-Silva, A. Amo, L. E. F. F. Torres, and R. A. Vicencio, Experimental observation of edge states in SSH-Stub photonic lattices, *Phys. Rev. Res.* **4**, 013185 (2022).
- [48] G. Cáceres-Aravena, B. Real, D. Guzmán-Silva, P. Vildoso, I. Salinas, A. Amo, T. Ozawa, and R. A. Vicencio, Edge-to-edge topological spectral transfer in diamond photonic lattices, *APL Photon.* **8**, 080801 (2023).
- [49] K. M. Davis, K. Miura, N. Sugimoto, and K. Hirao, Writing waveguides in glass with a femtosecond laser, *Opt. Lett.* **21**, 1729 (1996).
- [50] A. Szameit, D. Blömer, J. Burghoff, T. Schreiber, T. Pertsch, S. Nolte, A. Tünnermann, and F. Lederer, Discrete nonlinear localization in femtosecond laser written waveguides in fused silica, *Opt. Express* **13**, 10552 (2005).
- [51] D. Guzmán-Silva, G. Cáceres-Aravena, and R. A. Vicencio, Experimental observation of interorbital coupling, *Phys. Rev. Lett.* **127**, 066601 (2021).
- [52] D. Song, V. Paltoglou, S. Liu, Y. Zhu, D. Gallardo, L. Tang, J. Xu, M. Ablowitz, N. K. Efremidis, and Z. Chen, Unveiling pseudospin and angular momentum in photonic graphene, *Nat. Commun.* **6**, 6272 (2015).
- [53] J. Noh, W. A. Benalcazar, S. Huang, M. J. Collins, K. P. Chen, T. L. Hughes, and M. C. Rechtsman, Topological protection of photonic mid-gap defect modes, *Nat. Photon.* **12**, 408 (2018).
- [54] R. A. Vicencio and M. Johansson, Discrete gap solitons in waveguide arrays with alternating spacings, *Phys. Rev. A* **79**, 065801 (2009).
- [55] A. A. Sukhorukov, D. N. Neshev, and Y. S. Kivshar, Shaping and control of polychromatic light in nonlinear photonic lattices, *Opt. Express* **15**, 13058 (2007).
- [56] F. Dreisow, M. Heinrich, A. Szameit, S. Döring, S. Nolte, A. Tünnermann, S. Fahr, and F. Lederer, Spectral resolved dynamic localization in curved fs laser written waveguide arrays, *Opt. Express* **16**, 3474 (2008).
- [57] A. Szameit, I. L. Garanovich, M. Heinrich, A. A. Sukhorukov, F. Dreisow, T. Pertsch, S. Nolte, A. Tünnermann, and Y. S. Kivshar, Polychromatic dynamic localization in curved photonic lattices, *Nat. Phys.* **5**, 271 (2009).
- [58] A. Blanco-Redondo, I. Andonegui, M. J. Collins, G. Harari, Y. Lumer, M. C. Rechtsman, B. J. Eggleton, and M. Segev, Topological optical waveguiding in silicon and the transition between topological and trivial defect states, *Phys. Rev. Lett.* **116**, 163901 (2016).
- [59] L.-C. Wang, Y. Chen, M. Gong, F. Yu, Q.-D. Chen, Z.-N. Tian, X.-F. Ren, and H.-B. Sun, Edge state, localization length, and critical exponent from survival probability in topological waveguides, *Phys. Rev. Lett.* **129**, 173601 (2022).
- [60] F. Flamini, L. Magrini, A. S. Rab, N. Spagnolo, V. D' Ambrosio, P. Mataloni, F. Sciarrino, T. Zandrini, A. Crespi, R. Ramponi, and R. Osellame, Thermally reconfigurable quantum photonic circuits at telecom wavelength by femtosecond laser micromachining, *Light: Sci. Appl.* **4**, e354 (2015).
- [61] Y.-J. Chang, Y.-H. Lu, Y. Wang, X.-Y. Xu, W.-H. Zhou, W.-H. Cui, X.-W. Wang, J. Gao, L.-F. Qiao, and X.-M. Jin, Symmetry-induced error filtering in a photonic Lieb lattice, *Phys. Rev. Lett.* **126**, 110501 (2021).
- [62] G. Lifante Pedrola, *Beam Propagation Method for Design of Optical Waveguide Devices*, 1st ed. (Wiley & Sons, Hoboken, NJ, 2015).
- [63] K. Kawano and T. Kitoh, *Introduction to Optical Waveguide Analysis: Solving Maxwell's Equations and the Schrödinger Equation*, 1st ed. (Wiley & Sons, Hoboken, NJ, 2004).